Real-space finite-difference method for conductance calculations

Petr A. Khomyakov and Geert Brocks*
Computational Materials Science, Faculty of Science and Technology, and MESA$^+$ Research Institute, University of Twente, P. O. Box 217, 7500 AE Enschede, The Netherlands
(Received 7 May 2004; published 3 November 2004)

We present a general method for calculating coherent electronic transport in quantum wires and tunnel junctions. It is based upon a real-space high-order finite-difference representation of the single particle Hamiltonian and wave functions. Landauer's formula is used to express the conductance as a scattering problem. Dividing space into a scattering region and left and right ideal electrode regions, this problem is solved by wave function matching in the boundary zones connecting these regions. The method is tested on a model tunnel junction and applied to sodium atomic wires. In particular, we show that using a high-order finite-difference approximation of the kinetic energy operator leads to a high accuracy at moderate computational costs.

DOI: 10.1103/PhysRevB.70.195402 PACS number(s): 73.63.−b, 73.40.−c, 71.15.−m, 85.35.−p

I. INTRODUCTION

The progress in experimental control on the nanometer scale has enabled studies of electronic transport in quantum wires of atomic dimensions.[1] The transport properties of such systems have to be understood on the basis of their atomic structure. This notion has generated a large effort in recent years to calculate the conductance of quantum wires from first principles. Several different approaches have been formulated, which have a common basis in the Landauer-Büttiker approach to express the conductance of a coherent system in terms of a quantum mechanical scattering problem.[2] In such calculations the quantum wire consists of a scattering region of finite size, sandwiched between two semi-infinite leads that are considered to be ideal ballistic wires. Semiempirical tight-binding models have been exploited to solve this problem.[3–6] Aiming at a better description of the electronic structure, several current approaches rely upon density functional theory (DFT).

The main differences between these approaches lie in the approximations that are used to describe the atomic structure of the leads and in the techniques that are used to solve the scattering problem. In pioneering work, jellium (i.e., free electron) electrodes have been used to describe the leads and the scattering wave functions have been obtained by a transfer matrix method[7] or by solving the Lippman-Schwinger equation.[8,9] A transfer matrix method has also been used taking into account the full atomic structure of the leads at the DFT level.[10,11] Alternatively, the conductance can be calculated using a Green function approach without calculating the scattering wave functions explicitly.[12] Several implementations of this approach have been formulated that use a localized basis set to form a representation of the scattering problem. These implementations mainly differ in the kind of basis set used, e.g., Gaussian or numerical atomic orbitals, or wavelets.[13–19] An embedded Green function approach has been applied using a delocalized basis set of augmented plane waves.[20]

In this paper we present a technique for solving the scattering problem of a quantum wire without the use of a basis set. Instead, potentials and wave functions are represented on a uniform real-space grid and differential operators are approximated by a finite-difference approximation (FDA). Previous implementations of this idea have used a simple first order FDA.[21–24] In that case the grid has to be relatively fine in order to obtain sufficiently converged results. This hinders the application to large systems because of the computational costs involved in using fine grids. However, in ground state (DFT) electronic structure calculations high-order FDA's have been shown to markedly increase the efficiency of real-space grid techniques by enabling the use of coarse grids.[25–27] In this paper we demonstrate that high-order FDA's make it possible to solve the scattering problem much more efficiently.

The method we propose for calculating the conductance of a quantum wire is based upon wave function matching (WFM) in the boundary zones connecting the leads and the scattering region.[28] Unlike transfer matrix methods, however, it does not require the explicit calculation of wave functions in the scattering region.[7,10,11] It does not require the explicit calculation of Green functions either,[12–20] which enables us to solve the scattering problem at real, instead of complex, energies.[29] Our method can be classified as an $O(N)$ technique, since the computing costs are determined by the size of the scattering region with which they scale linearly. A related technique that uses a linearized muffin tin orbital basis set has been applied to calculate the electronic transport in layered magnetic materials.[30,31] Although the formalism presented here can be extended to the nonequilibrium situation, we consider in this paper the linear response regime only.

This paper is organized as follows. In Sec. II the main ingredients of our computational method are explained, where the computational details can be found in Appendix A. The accuracy and convergence properties of the method are verified on model tunnel junctions in Sec. III A. The application to a more complex system, which consists of a sodium atomic wire, is discussed in Sec. III B. A summary is given in Sec. IV.

II. COMPUTATIONAL METHOD

Within the Landauer-Büttiker approach the conductance G of a quantum wire is expressed in terms of the total transmission $T(E)$

$$G = \frac{e^2}{\pi\hbar} T(E), \tag{1}$$

assuming spin degeneracy.[2] $T(E)$ can be obtained by solving the quantum mechanical scattering problem at the fixed energy E. Equation (1) is valid in the linear response regime, where $T(E)$ needs to be evaluated at the Fermi energy $E = E_F$. Our quantum wire is defined as a system consisting of a finite scattering region that is connected left and right to semi-infinite leads. The latter are supposed to be "ideal" wires, which can be described by a periodic potential along the wire direction. In the scattering region the potential can have any shape. We consider two cases that can be treated by essentially the same technique. In the first case the system has a finite cross section perpendicular to the wire direction, whereas in the second case the system is periodic perpendicular to the wire. The latter case also covers planar interfaces and tunnel junctions.

In order to solve the scattering problem we generalize a method formulated by Ando.[28] Here one basically solves a single particle Schrödinger equation directly at a fixed energy E in two steps. In the first step one obtains the modes of the ideal leads. Subsequently the wave functions for the scattering region are constructed such that they are properly matched to the solutions in the leads. We use a real-space finite-difference method to represent the Schrödinger equation. In the following three subsections we will introduce this representation and discuss the steps required to solve the scattering problem.

A. Finite-difference approximation

We start from a single particle equation of the general form

$$\left(E - V(\mathbf{r}) + \frac{\hbar^2}{2m}\nabla^2\right)\Psi(\mathbf{r}) = 0, \tag{2}$$

which represents the Schrödinger equation of a single particle in a potential V. Alternatively, within the DFT scheme it represents the Kohn-Sham equation with V the total effective potential. We put the wave function Ψ and the potential V on a equidistant grid in real space $\mathbf{r}=(x_j,y_k,z_l)$, where $x_j = x_0 + jh_x$, $y_k = y_0 + kh_y$, $z_l = z_0 + lh_z$, and h_x, h_y, h_z are the grid spacings in the x, y, and z directions, respectively. Following Refs. 25 and 26 we replace the kinetic energy operator in Eq. (2) by a high-order FDA. For the x part this gives

$$\frac{\partial^2\Psi(x_j,y_k,z_l)}{\partial x^2} \approx \frac{1}{h_x^2}\sum_{n=-N}^{N} c_n \Psi(x_{j+n},y_k,z_l), \tag{3}$$

with similar expressions for the y and z parts. Expressions for the coefficients c_n for various values of N are tabulated in Ref. 26. The simplest approximation in Eq. (3) ($N=1$, where $c_1 = c_{-1} = 1$ and $c_0 = -2$) reduces Eq. (2) to the well-known simple finite difference representation of the Schrödinger equation.[12,21–24] However, we will demonstrate that the scattering problem can be solved much more efficiently using higher-order FDA's with $N=4-6$.

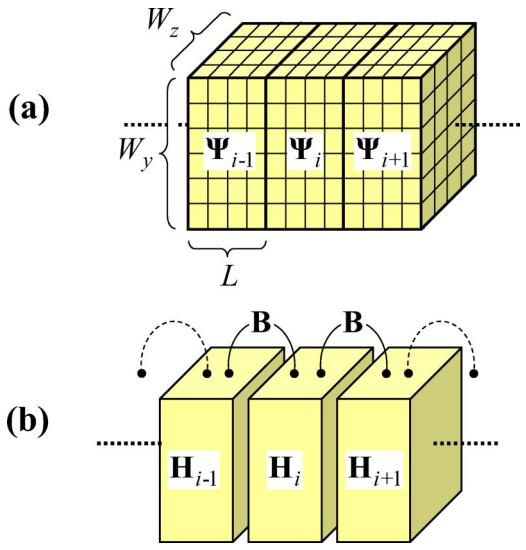

FIG. 1. (Color online) (a) The system is divided into cells indicated by an index i. The cells have L, W_y, and W_z grid points in the x, y, and z directions, respectively. $\mathbf{\Psi}_i$ is the supervector that contains the wave function values on all grid points in cell i. (b) $\mathbf{H}_i$ is the Hamilton matrix connecting grid points within cell i; the $\mathbf{B}$ matrix connects grid points between neighboring cells and is independent of i.

In a FDA the Schrödinger equation of Eq. (2) becomes

$$(E - V_{j,k,l})\Psi_{j,k,l} + \sum_{n=-N}^{N} (t_n^x \Psi_{j+n,k,l} + t_n^y \Psi_{j,k+n,l} + t_n^z \Psi_{j,k,l+n}) = 0, \tag{4}$$

where $V, \Psi_{j,k,l}$ is a shorthand notation for $V, \Psi(x_j,y_k,z_l)$ and $t_n^{x,y,z} = \hbar^2/2mh_{x,y,z}^2 \times c_n$. In order to make a connection to Ando's formalism[28] we divide the wire into cells of dimension $a_x \times a_y \times a_z$. The direction of the wire is given by the x axis. The number of grid points in a cell is $L = a_x/h_x$, $W_y = a_y/h_y$, and $W_z = a_z/h_z$ for the x, y, and z directions, respectively. We wish to distinguish between two different cases. In the first case the wire has a finite cross section in the yz plane. In the second case the wire has an infinite cross section, but it has a periodic potential in the yz plane, i.e., $V_{j,k+W_y,l} = V_{j,k,l+W_z} = V_{j,k,l}$. In both cases the (unit) cell in the yz plane is described by $W_y \times W_z$ grid points.

The values $\Psi_{j,k,l}$ where the indices j,k,l correspond to a single cell i are grouped into a supervector $\mathbf{\Psi}_i$. The idea is shown in Fig. 1. This supervector has the dimension $N_{\mathrm{rs}} = LW_yW_z$, which is the total number of real-space grid points in a cell. If we let i denote the position of the cell along the wire then Eq. (4) can be rewritten as

$$(E\mathbf{I} - \mathbf{H}_i)\mathbf{\Psi}_i + \mathbf{B}\mathbf{\Psi}_{i-1} + \mathbf{B}^\dagger\mathbf{\Psi}_{i+1} = 0 \tag{5}$$

for $i = -\infty, \ldots, \infty$. Here $\mathbf{I}$ is the $N_{\mathrm{rs}} \times N_{\mathrm{rs}}$ identity matrix. The matrix elements of the $N_{\mathrm{rs}} \times N_{\mathrm{rs}}$ matrices $\mathbf{H}_i$ and $\mathbf{B}$ can be

derived straightforwardly from Eq. (4). The expressions are given in Appendix A 1, both for a wire that is finite and for a wire that is periodic in the yz plane. For the latter $\mathbf{H}_i = \mathbf{H}_i(\mathbf{k}_\parallel)$, where $\mathbf{k}_\parallel$ is a wave vector in the two-dimensional Brillouin zone. In the following this notation is suppressed.

Equation (5) has the form of a nearest neighbor tight-binding equation, expressed in terms of vectors/matrices of dimension $N_{\rm rs}$. This form enables us to use Ando's technique to solve the scattering problem.[28] Note, however, that the matrices $\mathbf{B}, \mathbf{B}^\dagger$ in Eq. (4) are singular [see Eq. (A3)], which requires a generalization of this technique.

B. Ideal wire

An ideal wire is defined by a potential that is periodic in the direction of the wire, i.e., $V(x_j + a_x, y_k, z_l) = V(x_j, y_k, z_l)$ or $V_{j+L,k,l} = V_{j,k,l}$. Since the potential is the same in each cell, the matrix $\mathbf{H}_i = \mathbf{H}$ in Eq. (5) is independent of the cell position i. In a periodic system the vectors in subsequent cells are related by the Bloch condition

$$\lambda \mathbf{\Psi}_i = \mathbf{\Psi}_{i+1}, \tag{6}$$

where $\lambda = e^{ik_x a_x}$ with k_x real for propagating waves and complex for evanescent (growing or decaying) waves. Combining Eqs. (5) and (6) one then obtains the following generalized eigenvalue problem:

$$\left[\begin{pmatrix} E\mathbf{I} - \mathbf{H} & \mathbf{B} \\ \mathbf{I} & 0 \end{pmatrix} - \lambda \begin{pmatrix} -\mathbf{B}^\dagger & 0 \\ 0 & \mathbf{I} \end{pmatrix} \right] \begin{pmatrix} \mathbf{\Psi}_i \\ \mathbf{\Psi}_{i-1} \end{pmatrix} = 0. \tag{7}$$

Formally, the dimension of this problem is $2N_{\rm rs}$. There are a number of trivial solutions, however, since $\mathbf{B}, \mathbf{B}^\dagger$ are singular matrices. In Appendix A 2 it is shown how to reduce the problem to its $2NW_yW_z$ nontrivial solutions.

The nontrivial solutions of Eq. (7) can be divided into two classes. The first class comprises Bloch waves propagating to the right and evanescent waves decaying to the right; the corresponding eigenvalues are denoted by $\lambda(+)$. The second class comprises Bloch waves propagating to the left or evanescent waves decaying to the left; the eigenvalues are denoted by $\lambda(-)$. The eigenvalues of the propagating waves have $|\lambda(\pm)| = 1$ and for evanescent waves $|\lambda(\pm)| \lesseqgtr 1$. The evanescent states come in pairs, since it is easy to show that for every solution $\lambda(+)$ there is a corresponding solution $\lambda(-) = 1/\lambda^*(+)$. It can be shown that the propagating states also come in pairs, i.e., for every right propagating wave $\lambda(+)$ there is a left propagating wave $\lambda(-)$.[32]

It makes sense to keep only those evanescent waves for which $1/\delta < |\lambda| < \delta$, where δ is a sufficiently large number. States with $|\lambda|$ outside this interval are extremely fast decaying or growing. Such states are not important in matching an ideal wire to a scattering region. Typical of finite-difference schemes, there are also nonphysical solutions to Eq. (7), which are related to so-called parasitic modes.[33,34] These are easily recognized and discarded since their $|\lambda|$'s are either extremely small or large and thus fall outside the selected interval. Moreover, these $|\lambda|$'s are very sensitive to the grid spacing and rapidly go to 0 or ∞ if the grid spacing is decreased.

After filtering out the physical and useful solutions of Eq. (7) we end up with M pairs of solutions $\lambda_m(\pm)$, $m = 1, \ldots, M$, where usually $M \ll N_{\rm rs}$. We construct the normalized vectors $\mathbf{u}_m(\pm)$ from the first $N_{\rm rs}$ elements of the eigenvectors of Eq. (7) and form the $N_{\rm rs} \times M$ matrices

$$\mathbf{U}(\pm) = (\mathbf{u}_1(\pm) \cdots \mathbf{u}_M(\pm)). \tag{8}$$

Choosing the cell $i = 0$ as the origin, one then writes the general solution $\mathbf{\Psi}_0$ in this cell as a linear combination of these right and left going modes

$$\mathbf{\Psi}_0 = \mathbf{\Psi}_0(+) + \mathbf{\Psi}_0(-), \tag{9}$$

where

$$\mathbf{\Psi}_0(\pm) = \mathbf{U}(\pm)\mathbf{a}(\pm) = \sum_{m=1}^{M} \mathbf{u}_m(\pm) a_m(\pm), \tag{10}$$

with $\mathbf{a}(\pm)$ vectors of arbitrary coefficients of dimension M.

Defining the $M \times M$ diagonal eigenvalue matrices by

$$(\mathbf{\Lambda}(\pm))_{nm} = \delta_{nm} \lambda_m(\pm), \tag{11}$$

and using the Bloch condition of Eq. (6), the solution in the other unit cells then can be expressed in a compact form,

$$\mathbf{\Psi}_i = \mathbf{U}(+)\mathbf{\Lambda}^i(+)\mathbf{a}(+) + \mathbf{U}(-)\mathbf{\Lambda}^i(-)\mathbf{a}(-). \tag{12}$$

In order to apply Ando's formalism,[28] it is advantageous to slightly rewrite this. We define the $N_{\rm rs} \times N_{\rm rs}$ matrices $\mathbf{F}(\pm)$ and $\tilde{\mathbf{F}}(\pm)$ by

$$\mathbf{F}(\pm)\mathbf{U}(\pm) = \mathbf{U}(\pm)\mathbf{\Lambda}(\pm), \tag{13}$$

$$\tilde{\mathbf{F}}(\pm)\mathbf{U}(\pm) = \mathbf{U}(\pm)\mathbf{\Lambda}^{-1}(\pm). \tag{14}$$

Note that $\tilde{\mathbf{F}}(\pm) \neq \mathbf{F}^{-1}(\pm)$ since the $N_{\rm rs} \times M$ matrices $\mathbf{U}(\pm)$ are not square (typically $M \ll N_{\rm rs}$). This presents no problem, however, and explicit expressions for the matrices $\tilde{\mathbf{F}}, \mathbf{F}$ are given in Appendix A 3. They allow Eq. (12) to be rewritten in recursive form,

$$\mathbf{\Psi}_{i+1} = \mathbf{F}(+)\mathbf{\Psi}_i(+) + \mathbf{F}(-)\mathbf{\Psi}_i(-), \tag{15}$$

$$\mathbf{\Psi}_{i-1} = \tilde{\mathbf{F}}(+)\mathbf{\Psi}_i(+) + \tilde{\mathbf{F}}(-)\mathbf{\Psi}_i(-), \tag{16}$$

either of which allows one to construct the full solution for the ideal wire, once the boundary values are set [cf. Eq. (9)].

C. Scattering problem

In a nonideal quantum wire the potential is not periodic, which means that we have to solve the Schrödinger equation of Eq. (5) with $\mathbf{H}_i$ depending upon the position i along the wire. The nonideal region (the scattering region) is supposed to be finite, spanning the cells $i = 1, \ldots, S$.[35] The left and right leads are ideal wires, spanning the cells $i = -\infty, \ldots, 0$ and $i = S+1, \ldots, \infty$, respectively. In the ideal wires $\mathbf{H}_i$ does not depend on the position of the cell. However, the left lead can be different from the right one, so we use the subscript L (R) to denote the former (latter), i.e., $\mathbf{H}_i = \mathbf{H}_{\rm L}, i < 1$, and $\mathbf{H}_i$

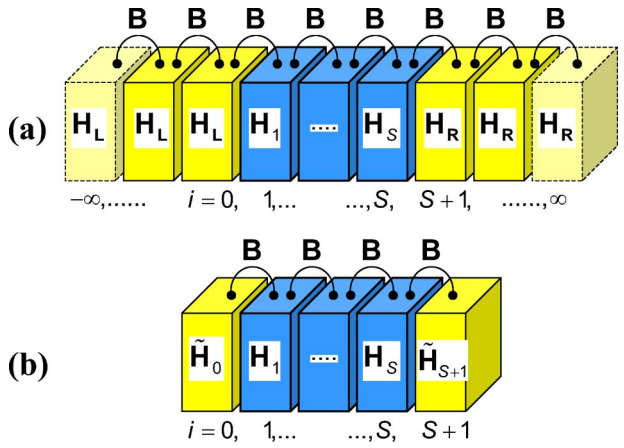

FIG. 2. (Color online) (a) Schematic representation of a quantum wire. The left (L) and right (R) leads are ideal wires that span the cells $i=-\infty,\ldots,0$ and $i=S+1,\ldots,\infty$, respectively. The scattering region spans cells $i=1,\ldots,S$. (b) The reduced problem spans the cells $i=0,\ldots,S+1$ [see Eq. (26)].

$=\mathbf{H}_R, i>S$. A schematic picture of the structure is shown in Fig. 2(a). We solve Eq. (5) over the whole space, $i=-\infty,\infty$, making use of the ideal wire solutions of the previous section to reduce the problem to essentially the scattering region only [see Fig. 2(b)].

For the solution in the left lead the recursion relation of Eq. (16) can be used. This gives for the cell $i=-1$

$$\begin{aligned}\boldsymbol{\Psi}_{-1} &= \tilde{\mathbf{F}}_L(+)\boldsymbol{\Psi}_0(+) + \tilde{\mathbf{F}}_L(-)\boldsymbol{\Psi}_0(-) \\ &= [\tilde{\mathbf{F}}_L(+) - \tilde{\mathbf{F}}_L(-)]\boldsymbol{\Psi}_0(+) + \tilde{\mathbf{F}}_L(-)\boldsymbol{\Psi}_0, \end{aligned} \tag{17}$$

using Eq. (9). The vector $\boldsymbol{\Psi}_0(+)$ describes a wave coming in from the left. In a scattering problem this vector fixes the boundary condition. Equation (17) allows Eq. (5) for $i=0$ to be written as

$$(E\mathbf{I} - \tilde{\mathbf{H}}_0)\boldsymbol{\Psi}_0 + \mathbf{B}^\dagger\boldsymbol{\Psi}_1 = \mathbf{Q}\boldsymbol{\Psi}_0(+), \tag{18}$$

where

$$\tilde{\mathbf{H}}_0 = \mathbf{H}_L - \mathbf{B}\tilde{\mathbf{F}}_L(-),$$

$$\mathbf{Q} = \mathbf{B}[\tilde{\mathbf{F}}_L(-) - \tilde{\mathbf{F}}_L(+)]. \tag{19}$$

For the solution in the right lead we use the recursion relation of Eq. (15), which gives for the cell $i=S+2$

$$\boldsymbol{\Psi}_{S+2} = \mathbf{F}_R(+)\boldsymbol{\Psi}_{S+1}(+). \tag{20}$$

Here we have assumed that in the right lead we have only a right going wave, which corresponds to the transmitted wave. Equation (20) allows Eq. (5) for $i=S+1$ to be written as

$$(E\mathbf{I} - \tilde{\mathbf{H}}_{S+1})\boldsymbol{\Psi}_{S+1} + \mathbf{B}\boldsymbol{\Psi}_S = 0, \tag{21}$$

where

$$\tilde{\mathbf{H}}_{S+1} = \mathbf{H}_R - \mathbf{B}^\dagger\mathbf{F}_R(+). \tag{22}$$

Equations (19) and (22) take care of the coupling of the scattering region to the left and right leads. Equation (5) for $i=1,\ldots,S$ plus Eqs. (18) and (21) form a complete set of equations from which the vectors $\boldsymbol{\Psi}_i, i=0,\ldots,S+1$, can be determined describing the waves in the scattering region.

The scattering reflection and transmission coefficients can be deduced from the amplitudes immediately left and right of the scattering region, i.e., $\boldsymbol{\Psi}_0$ and $\boldsymbol{\Psi}_{S+1}$. If we let the incoming wave consist of one specific mode, $\boldsymbol{\Psi}_0(+)=\mathbf{u}_{L,n}$, i.e., $a_m(+)=\delta_{mn}$ in Eq. (9), then the generalized reflection and transmission probability amplitudes $r_{n'n}$ and $t_{n'n}$ are defined by

$$\boldsymbol{\Psi}_0(-) = \sum_{n'=1}^{M_L} \mathbf{u}_{L,n'}(-)r_{n'n},$$

$$\boldsymbol{\Psi}_{S+1}(+) = \sum_{n'=1}^{M_R} \mathbf{u}_{R,n'}(+)t_{n'n}. \tag{23}$$

Note that at this stage we include all evanescent and propagating modes since these form a complete set to represent the states in the leads. We assume the lead states to be amplitude normalized.

The reflection and transmission probability amplitudes $r_{n'n}$ and $t_{n'n}$ between all possible modes form an $M_L \times M_L$ matrix $\mathbf{R}$ and an $M_R \times M_L$ matrix $\mathbf{T}$, respectively. All elements of these matrices can be found in one go by defining an $N_{rs} \times M_L$ matrix of all possible incoming modes, i.e.,

$$\mathbf{C}_0(+) = \mathbf{U}_L(+). \tag{24}$$

Analogous to Eq. (23) one then has

$$\mathbf{C}_0(-) = \mathbf{C}_0 - \mathbf{C}_0(+) = \mathbf{U}_L(-)\mathbf{R},$$

$$\mathbf{C}_{S+1}(+) = \mathbf{C}_{S+1} = \mathbf{U}_R(+)\mathbf{T}. \tag{25}$$

Equations (18), (5), and (21) then become

$$(E\mathbf{I} - \tilde{\mathbf{H}}_0)\mathbf{C}_0 + \mathbf{B}^\dagger\mathbf{C}_1 = \mathbf{Q}\mathbf{U}_L(+),$$

$$(E\mathbf{I} - \mathbf{H}_i)\mathbf{C}_i + \mathbf{B}\mathbf{C}_{i-1} + \mathbf{B}^\dagger\mathbf{C}_{i+1} = 0, \tag{26}$$

$$(E\mathbf{I} - \tilde{\mathbf{H}}_{S+1})\mathbf{C}_{S+1} + \mathbf{B}\mathbf{C}_S = 0,$$

$i=1,\ldots,S$. Solving this set of equations for $\mathbf{C}_i, i=0,\ldots,S+1$, gives all possible waves. From Eq. (25) one can then extract the generalized reflection and transmission matrices $\mathbf{R}$ and $\mathbf{T}$. An efficient technique for solving the equations is discussed in Appendix A 4.

In order to calculate the total transmission one has to select the transmission matrix elements that refer to propagating modes and discard the ones that refer to evanescent modes. This is easy, since the propagating modes have $|\lambda|=1$ [see the discussion above Eq. (8)]. The total transmission of Eq. (1) is then given by

$$T(E) = \sum_{n=1,n'=1}^{m_L,m_R} \frac{v_{R,n'}}{v_{L,n}} |t_{n'n}|^2, \tag{27}$$

where $v_{R,n'}$ and $v_{L,n}$ are the velocities in the x direction of the right propagating waves in the right and left leads in the modes n' and n, respectively, and m_L, m_R are the number of such modes. Introducing the velocities results from flux normalizing the modes, which is required by current conservation.[12] The velocities are given by the expression

$$v_n = -\frac{2a_x}{\hbar} \mathrm{Im}(\lambda_n \mathbf{u}_n^\dagger \mathbf{B}^\dagger \mathbf{u}_n), \tag{28}$$

where the subscripts L (R) need to be added for the left (right) leads. Equation (28) is derived in Appendix A 5. The sign of the calculated velocities is used to distinguish right from left propagating modes.

D. Computational costs

Our computational method can be summarized as follows. First, Eq. (7) is solved in its reduced form, Eq. (A8), to obtain the modes for both leads. The computing costs of this step scale as N_{id}^3, where $N_{id}=\max(2N, L-N)\times W_y W_z$ (see Appendix A 2). These costs are small compared to the costs of solving the scattering problem. The next step involves selecting the physically relevant modes $\mathbf{u}_m$ and separating them into left (+) and right (−) going modes. The velocities are calculated using Eq. (28) and are used to distinguish left from right propagating states. Evanescent states are classified as growing (+) or decaying (−) on account of their eigenvalue. Subsequently, the **F** matrices are constructed, Eq. (13), and the matrix elements that define the boundary conditions on the scattering region are set [see Eqs. (19) and (22)]. The computing costs of these steps are minor.

The transmission matrix **T** is obtained by solving Eq. (26) using the algorithm of Appendix A 4. This is the most time consuming step. It scales as SN_{rs}^3, where $N_{rs}=LW_yW_z$ is the number of grid points in the unit cell and S is the number of unit cells in the scattering region. Note that the scaling is linear with respect to the size S of the scattering region, which means that this algorithm can be classified as $O(N)$. Finally, the total transmission and the conductance can be obtained from Eqs. (27) and (1).

III. RESULTS

A. Numerical tests

In order to test the accuracy of our method we consider a system described by the model potential

$$V(\mathbf{r}) = V_0[\cos(2\pi x/a) + \cos(2\pi y/a) + \cos(2\pi z/a)] + \frac{V_1}{\cosh^2(\pi x/a)}. \tag{29}$$

The V_0 term describes an ideal wire by a simple three dimensional periodic potential with periods $a_x=a_y=a_z=a$. The V_1 term describes a barrier in the propagation direction and is a simple model for a tunnel junction. The potential is plotted in

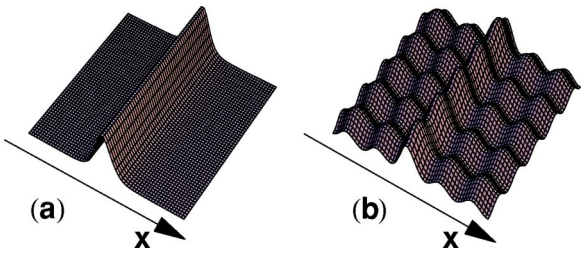

FIG. 3. (Color online) The potential of Eq. (29) in the xy plane for the cases (a) $V_0=0$ and (b) $V_0=V_1$.

Fig. 3. We solve the scattering problem for this system numerically in three dimensions by the method outlined in Sec. II. Our results can be verified, however, since this potential is in fact separable and limiting cases can be solved analytically. The solutions in the y and z directions are Mathieu functions.[36] If $V_1=0$ then the solutions in the x direction are also Mathieu functions. If $V_1\neq 0$ but $V_0=0$ the scattering problem can be solved analytically.[37] Finally, if $V_1\neq 0$ and $V_0\neq 0$ the solution in the x direction can be obtained using the separability of the potential and a standard numerical solver for the resulting ordinary differential equation in the x direction.[38] In the following the latter will be called the "exact" numerical solution.

As a first test we consider an ideal wire, i.e., $V_1=0$ in Eq. (29). The potential is separable and we can write the energy as $E(k_x,k_y,k_z)=\epsilon_{n_x}(k_x)+\epsilon_{n_y}(k_y)+\epsilon_{n_z}(k_z)$, where $\epsilon_n(k)$, $k=-\pi/a,\ldots,\pi/a$, $n=0,1,\ldots$, are the eigenvalues of the Mathieu problem.[36] Figure 4 shows part of the analytical band structure for $(k_x,k_y,k_z)=(0,0,0)\rightarrow(\pi/a,0,0)$. It essentially consists of a superposition of one-dimensional band structures $\epsilon_{n_x}(k_x)$ offset by energies $\epsilon_{n_y}(0)+\epsilon_{n_z}(0)$, n_y, $n_z=0,1,\ldots$.

The numerical band structure is obtained by solving Eq. (7) in its reduced form, Eq. (A8). To obtain the results shown in Fig. 4 we set $\mathbf{k}_\parallel=(k_y,k_z)=(0,0)$ [cf. Eq. (A4)], and determine the eigenvalues λ in Eq. (7) as a function of E. For the

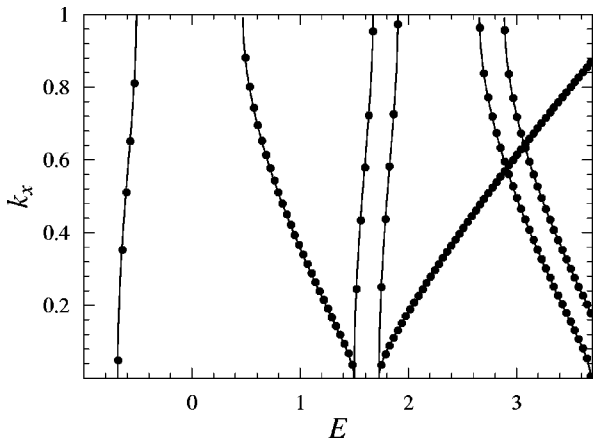

FIG. 4. The calculated wave number k_x (in units of π/a) as function of the energy E (in units of V_0) for an ideal wire. The points indicate the numerical results obtained with L, W_y, $W_x=8$ and $N=4$. The solid line indicates the exact solution of the Mathieu problem.

TABLE I. $k_x(E)$ (in units of π/a) at values of E (in units of V_0) in the lowest two bands and in the first band gap of Fig. 4; in the band gap we find $k_x=1+i\kappa_x$.

N	L	$k_x(-0.6)$	$k_x(1.0)$	$\kappa_x(0.3)$
1	7	0.694906	0.283091	0.283549
	10	0.608958	0.322712	0.304238
	14	0.571387	0.342011	0.312259
	100	0.533341	0.359187	0.319658
	1000	0.533084	0.359425	0.319688
4	5	0.544347	0.355049	0.317777
	7	0.533962	0.358927	0.319476
	10	0.533149	0.359389	0.319673
	14	0.533087	0.359425	0.319687
6	7	0.533228	0.359337	0.319658
	10	0.533086	0.359425	0.319688
	14	0.533082	0.359428	0.319688
Exact		0.533082	0.359428	0.319688

propagating states one can write $\lambda=\exp(ik_xa)$. Plotting the calculated wave number k_x as function of the energy E then allows us to compare the results with the analytical band structure. The numerical results shown in Fig. 4 are obtained using a grid of L, W_y, $W_z=8$ points per period and a FDA with $N=4$. Although this grid is relatively coarse, we obtain a relative accuracy on k_x of 10^{-3}.

This perhaps surprising accuracy is entirely due to the use of a high-order FDA. To illustrate this, Table I shows the convergence of k_x at a number of energies E as a function of the order N of the FDA and the number of grid points L. These particular results were obtained using the separability of the potential and solving the problem numerically in the x direction only, while using analytical solutions for the y and z directions. For $N=6$ and $L=14$ the results are converged to within 10^{-7} of the exact result. This is in sharp contrast to the results obtained with a simple first order ($N=1$) FDA, where a similar convergence can only be obtained at the cost of using two orders of magnitude more grid points. Using such a large number of grid points in three dimensions is entirely prohibitive because of the high computational costs involved. For example, aiming at a moderate accuracy of 10^{-2}, it is observed that for $N=4$ and $L=5$ the results are markedly better than for $N=1$ and $L=14$. Yet in a three-dimensional calculation, without using the separability of the potential, the computing time required for the latter is two orders of magnitude larger than for the former. It means that in order to solve a general nonseparable three-dimensional problem with reasonable accuracy and computational costs, it is vital to use a high-order FDA.

Next we consider the scattering problem and calculate the total transmission for the case where $V_1\neq 0$. The size of the scattering region is set to Sa and outside this region the scattering potential [the last term of Eq. (29)] is set to zero. With $S=6$ the results are extremely well converged. As an example we have calculated the transmission at normal incidence, i.e., $\mathbf{k}_\parallel=(k_y,k_z)=(0,0)$. The crosses marked $V_0=0$ in Fig. 5 represent the numerical results for the transmission of

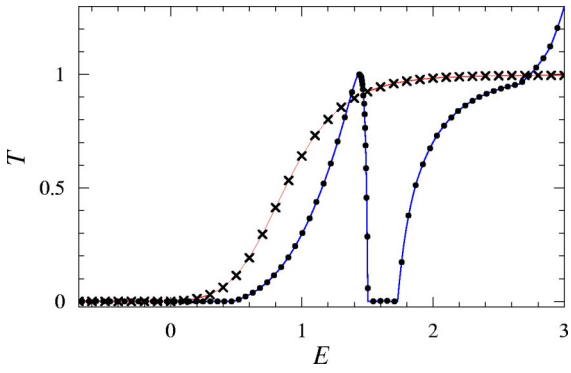

FIG. 5. (Color online) The total transmission as a function of energy (in units of V_1) for the two cases $V_0=0$ (crosses) and $V_0=V_1$ (dots). In both cases $\mathbf{k}_\parallel=(0,0)$. The solid lines represent the analytical solution for $V_0=0$ and the "exact" numerical solution for $V_0=V_1$.

the corresponding potential, obtained with an L, W_y, $W_z=8$ grid and a $N=4$ FDA. This scattering problem can also be solved analytically,[37] and the analytical and numerical transmission probabilities agree within 10^{-4}.

Figure 5 also shows the transmission for the case where $V_0=V_1$, as calculated numerically using the same parameters as before, i.e. $S=6$; L, W_y, $W_z=8$; $N=4$. This scattering problem can be solved only semianalytically; Mathieu solutions are used in the y and z directions, and the (ordinary) differential equation for the x direction is solved "exactly" using an accurate standard numerical solver.[38] Again the "exact" and numerical transmission probabilities agree within 10^{-4}. Compared to the $V_0=0$ case it is observed that the influence of the periodic potential of the leads upon the transmission is large. For $V_0=V_1$ the electronic states in the leads are far from free-electron-like (see Fig. 4). In particular, the transmission drops to zero if the energy is inside a band gap, because there are no lead states of that energy.

The numerical calculations accurately capture the transmission curve over a large energy range, as is shown in Fig. 6. The transmission generally increases with energy due to the increasing number of channels (see Fig. 4). Since the density of states peaks at the band edges, the transmission

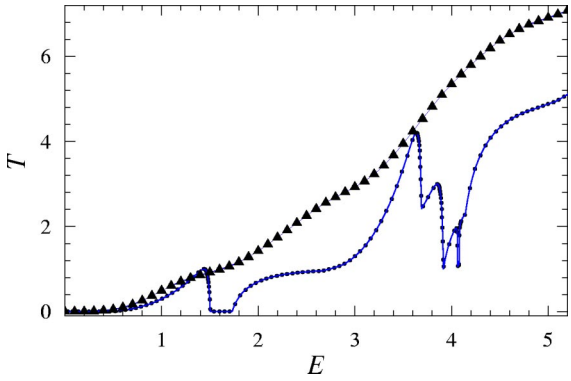

FIG. 6. (Color online) The total transmission as a function of energy (in units of V_1) for the two cases $\mathbf{k}_\parallel=(0,0)$ (dots) and $\mathbf{k}_\parallel=(0.47,0.21)\pi/a$ (triangles). In both cases $V_0=V_1$. The solid lines represent the "exact" numerical solution.

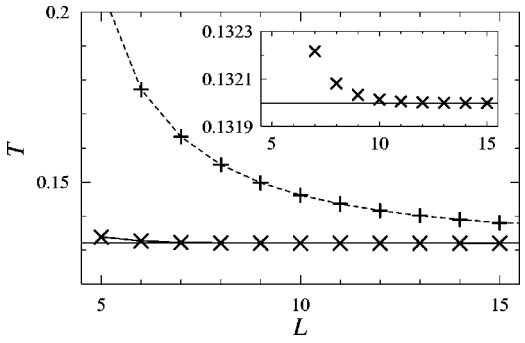

FIG. 7. The total transmission T as a function of the grid size $L=W_y=W_z$ for a simple $N=1$ FDA, + top curve; and for a $N=4$ FDA, × bottom curve. The horizontal line represents the "exact" value $T=0.132$. The inset shows the $N=4$ curve on a finer scale for T.

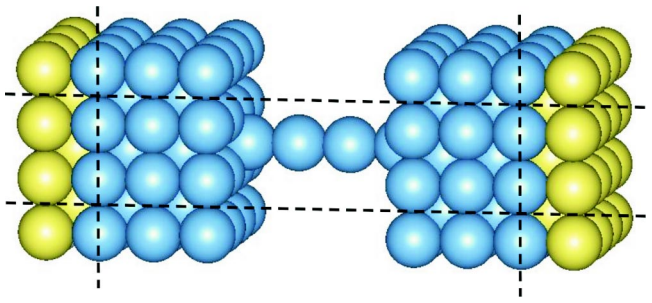

FIG. 8. (Color online) Structure of an atomic wire consisting of four sodium atoms between two sodium leads terminated by (100) surfaces. The scattering region is bounded by the vertical lines and the lateral supercell by the horizontal lines. Bulk atoms are indicated by light gray (yellow) balls and atoms in the scattering region by dark gray (blue) balls.

peaks at the corresponding energies. The transmission depends very much upon $\mathbf{k}_\parallel$ as can be observed in Fig. 6, where the transmission for normal incidence, $\mathbf{k}_\parallel=(0,0)$, can be compared to that for $\mathbf{k}_\parallel=(0.47,0.21)\pi/a$ (an arbitrary point in the Brillouin zone). The difference between the two curves can be easily understood from the band structure of the leads. In particular, for $\mathbf{k}_\parallel=(0.47,0.21)\pi/a$ there are no band gaps for $E>0.14V_0$.

To demonstrate the convergence of the numerical calculations, Fig. 7 shows the total transmission as function of the sampling density $L=W_y=W_z$ for a simple $N=1$ and a high-order $N=4$ FDA. The results shown are for one particular $\mathbf{k}_\parallel=(k_y,k_z)=(0.47,0.21)\pi/a$ and energy $E=0.895V_0$, but the convergence at other $\mathbf{k}_\parallel$ points and energies is very similar. The number of propagating channels at this $\mathbf{k}_\parallel$ point and energy is two, but the total transmission is only $T=0.132$, which means that the barrier is largely reflecting. We conclude that the accuracy of the three-dimensional calculation depends very strongly upon the order of the FDA. For $N=1$, $L=15$, the transmission is converged on a scale of 10^{-2} only, but for $N=4$ it is converged on a scale of 10^{-3} already for $L=8$ (see the inset of Fig. 7). A high-order FDA thus enables the use of a much coarser real-space grid. Since the computational costs scale with the number of real-space grid points $N_{\rm rs}$ as $N_{\rm rs}^3=L^9$, this demonstrates the strength of using a high-order FDA.

B. Sodium atomic wires

We have calculated the electronic transport in sodium atomic wires as examples of more complex systems. Our model of a sodium wire consists of left and right leads composed of bulk (bcc) sodium metal terminated by a (100) surface, connected by a straight wire of sodium atoms, as is shown in Fig. 8. The atoms in the leads are positioned according to the bcc structure of bulk sodium, with the cell parameter fixed at the experimental value of $7.984a_0$.[39] The atoms in the wire are fixed at their (bulk) nearest neighbor distance of $6.915a_0$. Since geometry relaxation at the Na(100) surface is very small,[40] and calculations using jellium electrodes have shown that the conductance of a sodium wire is not very sensitive to its geometry,[41] we have refrained from optimizing the geometry. Perpendicular to the wire we apply periodic boundary conditions using a 2×2 lateral supercell, which has a lattice parameter of $15.968a_0$.

If DFT is used to model the electronic structure, Eq. (2) corresponds to the Kohn-Sham equation. The one-electron potential $V(\mathbf{r})$ in this equation is then given by the sum of the nuclear Coulomb potentials or pseudopotentials, and the electronic Hartree and exchange-correlation potentials. The latter two depend upon the electronic charge density. In linear response the charge density remains that of the ground state, allowing the electronic potentials to be obtained from a self-consistent ground state calculation. In these calculations we employ supercells containing a slab of 13 layers to represent the bulk and surface of the leads, and a wire of n atoms (see Fig. 8). We use the local density approximation,[42] and represent the ion cores of the sodium atoms by a local pseudopotential.[43] The valence electronic wave functions are expanded in a plane wave basis set with a kinetic energy cutoff of 16 Ry. The lateral Brillouin zone is sampled with an 8×8 $\mathbf{k}_\parallel$-point grid, using a temperature broadening with $kT_{el}=0.1$ eV.[44]

We want to calculate the conductance for various lengths of the atomic wire, so for each length n we perform a self-consistent supercell calculation to generate the one-electron potential. By expressing the latter in a plane wave basis, Fourier interpolation can be used to obtain a representation on any real-space grid required for the transport calculations [cf. Eq. (4)]. An example of the effective potential for valence electrons of a sodium atomic wire is shown in Fig. 9.

For the transport calculations we use a scattering region comprising the atomic wire and the surface regions of the left and right leads. Both surface regions consist of five atomic layers (see Fig. 8). Periodic boundary conditions and a 2×2 lateral supercell perpendicular to the wire are applied. The potential in the scattering region is extracted from the slab calculations. Outside the scattering region we assume that the leads consist of bulk sodium. The potential for the leads and the value of the Fermi energy are extracted from a bulk calculation. The average bulk potential is lined up with the average potential in the middle of the supercell slab.[45] We have checked that the spatial dependence of the bulk

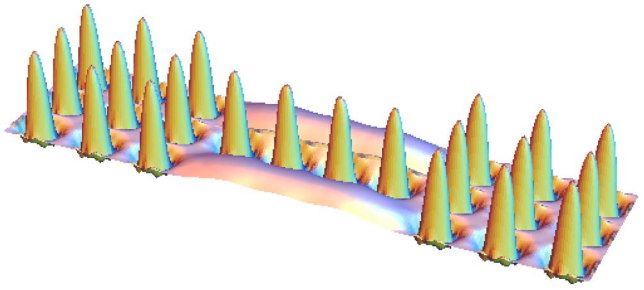

FIG. 9. (Color online) The effective potential for valence electrons in the *xy* plane of the sodium atomic wire shown in Fig 8. Most prominent are the strongly repulsive core regions and the attractive valence regions of the atoms. The difference between the maximum and minimum values of this potential is 32.4 eV. The Fermi level is at 8.5 eV above the potential minimum.

potential is virtually identical to that of the potential in the middle of the slab. This means that the connection between the leads and the scattering region is smooth. There are no discontinuities in the potential in the boundary regions that could cause spurious reflections.

Figure 10 shows the calculated conductance $G(E_F)$ at the Fermi level as a function of the length n of the sodium atomic wire. The conductance is calculated using a grid spacing along the x, y, and z directions of $h_{x,y,z}=0.67a_0$ (giving $L=6$, $W_y=W_z=24$) and a FDA of order $N=4$.[46] The 2×2 lateral Brillouin zone is sampled by a 12×12 uniform $\mathbf{k}_\parallel$-point grid. With these parameters the calculated conductances have converged to well within $10^{-3}G_0$ [where $G_0=e^2/(\pi\hbar)$].[47] All wires have a conductance close to unity, except the one-atom ($n=1$) wire. The high conductance for the one-atom wire is foremost due to tunneling between the left and right leads through vacuum. The latter can be calculated by omitting the wire and otherwise keeping the geometry fixed. Tunneling through vacuum leads to a conductance of $2.20G_0$ per 2×2 surface cell. Vacuum tunneling decreases fast with the distance between left and right lead surfaces. At

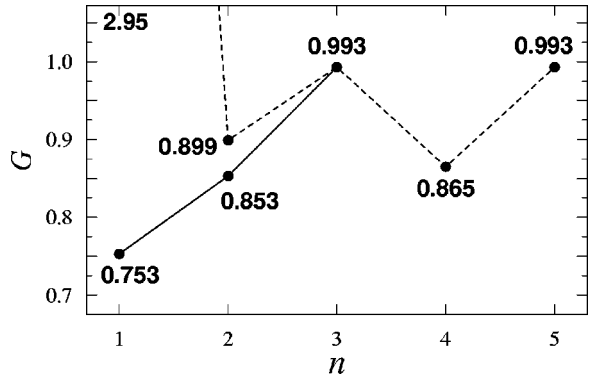

FIG. 10. Top curve: Conductance $G(E_F)$ at the Fermi level (in units of $e^2/\pi\hbar$) of a sodium atomic wire as a function of the number of atoms n in the wire. Bottom curve: Conductance of a sodium atomic wire relative to vacuum tunneling conductance between two electrodes without wire.

a distance corresponding to the two-atom wire it gives a conductance of $0.047G_0$; at distances corresponding to longer wires this conductance is negligible. Subtracting these vacuum tunneling values gives the lower curve in Fig. 10.

With the exception of the one-atomic wire, the conductances are close to unity. This is perhaps not surprising, since within a tight-binding model atomic wires consisting of a monovalent atom like sodium are expected to have one open channel. For perfectly transmitting contacts this would give a conductance of $1G_0$.[48] Our calculated conductances for $n>1$ are less than 15% smaller than this value, demonstrating that this transmission is indeed very high. The conductance of the one-atomic wire, relative to the vacuum tunneling conductance at this distance, is significantly lower than unity. The electronic structure of a single atom between two electrodes is substantially distorted from the simple single open channel model.[8]

On a finer scale we find evidence of an even-odd oscillation in the conductance obtained in previous studies.[8,49–52] The conductance for wires with n even tends to be lower than for those with n odd. In simple tight-binding terms odd-numbered atomic wires have a nonbonding level that tends to line up with the Fermi level of the leads, which gives a high transmission. For an even-numbered atomic wire, on the other hand, the Fermi level tends to fall in the gap between the bonding and antibonding levels of the wire, resulting in a lower transmission.[53] The size of the even-odd oscillation in the conductance depends of course upon the nature of the contacts between the atomic wire and the leads. Good contacts broaden the levels of the atomic wire into wide resonances, which tends to suppress the even-odd oscillation. Our wires have good contacts, but the even-odd oscillation remains distinctly visible.[54]

IV. SUMMARY

We have formulated and implemented a numerical technique for calculating electronic transport in quantum wires and tunnel junctions in the linear response regime, starting from Landauer's scattering formalism. It is based upon a real-space grid representation of the scattering problem. Dividing space into left and right ideal leads and a scattering region, the problem is solved by *wave function matching*. First all propagating and evanescent Bloch modes of the leads are calculated. Subsequently the states in the scattering region are forced to match to the Bloch modes of the leads. This directly leads to the transmission matrix, which contains the transmission probability amplitudes between all modes of the left and right leads, and to the conductance. The computing costs of this algorithm scale linearly with the size of the scattering region.

It is shown that the use of a high-order finite-difference approximation for the kinetic energy operator leads to a high accuracy and efficiency. This is demonstrated for a model potential by benchmarking the technique against analytical and numerically "exact" solutions. The method is then applied to calculate the conductance in sodium atomic wires, where the potential in the wire and in the bulk sodium leads is obtained from self-consistent DFT calculations.

ACKNOWLEDGMENTS

The authors acknowledge helpful discussions with P. J. Kelly and M. Zwierzycki. The work of P.A.K. is financially supported by a grant from the "Nederlandse Organisatie voor Wetenschappelijk Onderzoek (NWO), gebied Chemische Wetenschappen (CW)." The work of G.B. is part of the research program of the "Stichting voor Fundamenteel Onderzoek der Materie (FOM)," financially supported by NWO. The "Stichting Nationale Computerfaciliteiten (NCF)" is acknowledged for granting computer time.

APPENDIX A: COMPUTATIONAL DETAILS

1. H and B matrices

In this section the matrices $\mathbf{H}_i$ and $\mathbf{B}$, introduced in Sec. II A, are presented explicitly. In order not to complicate the notation the subscript i is dropped; all quantities refer to a single cell. For a wire with a finite cross section in the yz plane, the matrix $\mathbf{H}$ is real and symmetric and has the form

$$\mathbf{H}=\begin{pmatrix} \mathbf{h}_1 & -\boldsymbol{\beta}_1 & \dots & -\boldsymbol{\beta}_N & 0 & \dots & 0 & 0 \\ -\boldsymbol{\beta}_1 & \mathbf{h}_2 & \dots & -\boldsymbol{\beta}_{N-1} & -\boldsymbol{\beta}_N & \dots & 0 & 0 \\ \vdots & \vdots & \vdots & \vdots & \vdots & \vdots & \vdots & \vdots \\ 0 & 0 & \dots & 0 & 0 & \dots & \mathbf{h}_{L-1} & -\boldsymbol{\beta}_1 \\ 0 & 0 & \dots & 0 & 0 & \dots & -\boldsymbol{\beta}_1 & \mathbf{h}_L \end{pmatrix}. \tag{A1}$$

Here N is the order of the finite-difference formula used [see Eq. (3)]. We assume that the x axis is in the direction of the wire. L is the number of grid points in the x direction of the unit cell defined by the periodic potential.

The submatrices $\mathbf{h}_n$ and $\boldsymbol{\beta}_n$ are of dimension $W_y \times W_z$, which is the number of grid points in the cross section of the wire. Denoting $(k,l)=k+(l-1)W_y$, $k=1,\dots,W_y$, $l=1,\dots,W_z$, as the compound index covering the grid points in the cross section, the nonzero elements of these matrices are easily derived from Eq. (4):

$$(\mathbf{h}_j)_{(k,l),(k,l)} = V_{j,k,l} - (t_0^x + t_0^y + t_0^z),$$

$$(\mathbf{h}_j)_{(k,l),(k+n,l)} = -t_n^y, \quad n \neq 0,$$

$$(\mathbf{h}_j)_{(k,l),(k,l+n')} = -t_{n'}^z, \quad n' \neq 0,$$

$$(\boldsymbol{\beta}_j)_{(k,l),(k,l)} = t_j^x, \tag{A2}$$

where $-N \leqslant n,n' \leqslant N$ and $1 \leqslant k,k+n \leqslant W_y$, $1 \leqslant l,l+n' \leqslant W_z$, $1 \leqslant j \leqslant N$. Note that in writing down these matrices we have assumed that $N < L$, W_y, W_z. In practical calculations on realistic systems this will always be the case.

The matrix $\mathbf{B}$ has the same dimension as $\mathbf{H}$, but it is upper triangular:

$$\mathbf{B}=\begin{pmatrix} 0 & \dots & 0 & \boldsymbol{\beta}_N & \boldsymbol{\beta}_{N-1} & \dots & \boldsymbol{\beta}_1 \\ 0 & \dots & 0 & 0 & \boldsymbol{\beta}_N & \dots & \boldsymbol{\beta}_2 \\ \vdots & \vdots & \vdots & \vdots & \vdots & \vdots & \vdots \\ 0 & \dots & 0 & 0 & 0 & \dots & \boldsymbol{\beta}_N \\ \vdots & \vdots & \vdots & \vdots & \vdots & \vdots & \vdots \\ 0 & \dots & 0 & 0 & 0 & \dots & 0 \end{pmatrix}. \tag{A3}$$

For a wire that is periodic in the yz plane, the wave functions in Eq. (4) must obey Bloch conditions. That is, $\Psi_{j,k+W_{y,l}} = e^{ik_y a_y}\Psi_{j,k,l}$ and $\Psi_{j,k,l+W_z} = e^{ik_z a_z}\Psi_{j,k,l}$, where a_y, a_z are the periods in the y and z directions, and $(k_y,k_z)=\mathbf{k}_\parallel$ is the Bloch wave vector in the yz plane. These Bloch conditions in the yz plane can be taken into account by defining the blocks

$$(\mathbf{h'}_j)_{(k,l),(k+W_y+n,l)} = -t_n^y e^{-ik_y a_y}, \quad n=-N,\dots,-k,$$

$$(\mathbf{h'}_j)_{(k,l),(k-W_y+n,l)} = -t_n^y e^{ik_y a_y}, \quad n=W_y-k,\dots,N,$$

$$(\mathbf{h'}_j)_{(k,l),(k,l+W_z+n')} = -t_{n'}^z e^{-ik_z a_z}, \quad n'=-N,\dots,-l,$$

$$(\mathbf{h'}_j)_{(k,l),(k,l-W_z+n')} = -t_{n'}^z e^{ik_z a_z}, \quad n'=W_z-l,\dots,N. \tag{A4}$$

The matrix $\mathbf{H}(\mathbf{k}_\parallel)$, which is obtained by substituting $\mathbf{h}_j$ by $\mathbf{h}_j+\mathbf{h}'_j$, $j=1,\dots,L$, in Eq. (A1), describes a wire that is periodic in the yz plane with solutions corresponding to a Bloch vector $\mathbf{k}_\parallel$. This matrix is (complex) Hermitian.

2. Ideal wire

For an ideal wire, which has a periodic potential along the wire, Eq. (7) has to be solved to find the propagating and the evanescent waves. The precise form of the submatrices in Eqs. (A1) and (A3) is not important in the following discussion. For ease of notation we mention only the dimensions L (the number of grid points in the x direction) and N (the order of the finite-difference expression) explicitly and treat the wire as quasi-one-dimensional. To find the dimensions of the matrices in the three-dimensional case, one simply has to multiply the dimensions mentioned below by $W_y \times W_z$.

Equation (7) is a generalized eigenvalue problem of dimension $2L$. Because the matrix $\mathbf{B}$ is singular it has a number of trivial solutions $\lambda=0$ and $\lambda=\infty$. By using a partitioning technique we will eliminate these trivial solutions and reduce the problem to the $2N$ nontrivial solutions. The key point is to split the vectors $\boldsymbol{\Psi}_i$ into two parts containing the first $L-N$ and last N elements, respectively. The two parts are denoted by the subscripts 1 and 2. Splitting the matrices $\mathbf{H}$ and $\mathbf{B}$ in the same way one gets

$$\boldsymbol{\Psi}_i=\begin{pmatrix}\boldsymbol{\Psi}_{i,1}\\ \boldsymbol{\Psi}_{i,2}\end{pmatrix}, \quad \mathbf{H}=\begin{pmatrix}\mathbf{H}_{11} & \mathbf{H}_{12}\\ \mathbf{H}_{21} & \mathbf{H}_{22}\end{pmatrix}, \quad \mathbf{B}=\begin{pmatrix}0 & \mathbf{B}_{12}\\ 0 & \mathbf{B}_{22}\end{pmatrix}. \tag{A5}$$

Note the special form of the matrix **B**.

This splitting allows Eq. (7) to be written in the form

$$\begin{pmatrix} E\mathbf{I}_{11}-\mathbf{H}_{11} & -\mathbf{H}_{12} & 0 & \mathbf{B}_{12} \\ -\mathbf{H}_{21}+\lambda\mathbf{B}_{21}^{\dagger} & E\mathbf{I}_{22}-\mathbf{H}_{22}+\lambda\mathbf{B}_{22}^{\dagger} & 0 & \mathbf{B}_{22} \\ \mathbf{I}_{11} & 0 & -\lambda\mathbf{I}_{11} & 0 \\ 0 & \mathbf{I}_{22} & 0 & -\lambda\mathbf{I}_{22} \end{pmatrix} \times \begin{pmatrix} \boldsymbol{\Psi}_{i,1} \\ \boldsymbol{\Psi}_{i,2} \\ \boldsymbol{\Psi}_{i-1,1} \\ \boldsymbol{\Psi}_{i-1,2} \end{pmatrix} = 0. \tag{A6}$$

From this expression it is clear that the component $\boldsymbol{\Psi}_{i-1,1}$ enters the problem only in a trivial way as $\boldsymbol{\Psi}_{i-1,1}=1/\lambda \times \boldsymbol{\Psi}_{i,1}$. It can be eliminated by deleting the third row and column in Eq. (A6).

Furthermore, the first row of the matrix does not depend upon the eigenvalue λ. Writing out the multiplication for the first row explicitly, one finds an expression for $\boldsymbol{\Psi}_{i,1}$,

$$\boldsymbol{\Psi}_{i,1} = (E\mathbf{I}_{11}-\mathbf{H}_{11})^{-1}(\mathbf{H}_{12}\boldsymbol{\Psi}_{i,2}-\mathbf{B}_{12}\boldsymbol{\Psi}_{i-1,2}). \tag{A7}$$

This can be used to eliminate $\boldsymbol{\Psi}_{i,1}$ from Eq. (A6) to arrive at the equation

$$\left[\begin{pmatrix} \mathbf{A}_{11} & \mathbf{A}_{12} \\ \mathbf{I}_{22} & 0 \end{pmatrix} - \lambda \begin{pmatrix} \mathbf{S}_{11} & \mathbf{S}_{12} \\ 0 & \mathbf{I}_{22} \end{pmatrix}\right] \begin{pmatrix} \boldsymbol{\Psi}_{i,2} \\ \boldsymbol{\Psi}_{i-1,2} \end{pmatrix} = 0, \tag{A8}$$

with

$$\begin{aligned} \mathbf{A}_{11} &= E\mathbf{I}_{22}-\mathbf{H}_{22}-\mathbf{H}_{21}(E\mathbf{I}_{11}-\mathbf{H}_{11})^{-1}\mathbf{H}_{12}, \\ \mathbf{A}_{12} &= -\mathbf{H}_{21}(E\mathbf{I}_{11}-\mathbf{H}_{11})^{-1}\mathbf{B}_{12}, \\ \mathbf{S}_{11} &= -\mathbf{B}_{22}^{\dagger}-\mathbf{B}_{21}^{\dagger}(E\mathbf{I}_{11}-\mathbf{H}_{11})^{-1}\mathbf{H}_{12}, \\ \mathbf{S}_{12} &= -\mathbf{B}_{21}^{\dagger}(E\mathbf{I}_{11}-\mathbf{H}_{11})^{-1}\mathbf{B}_{12}. \end{aligned} \tag{A9}$$

Equation (A8) is a generalized eigenvalue problem of dimension $2N$ that can be solved using standard numerical techniques.[55] In general it gives $2N$ eigenvalues λ_m and eigenvectors $\mathbf{u}_m$. As mentioned in the text, some of these solutions are nonphysical;[33,34] others represent extremely fast growing or decaying waves. Both of these classes of unwanted solutions are easily filtered out by demanding that $1/\delta<|\lambda|<\delta$, where δ is some threshold value. We use this criterion to select the physically relevant solutions, which are then separated into M right going and M left going solutions. These are used to construct the matrices of Eqs. (8) and (11) which contain all the information required to describe the ideal wire.

The computational cost of solving Eq. (A8) scales as $(2N)^3$, whereas the cost of computing the matrices of Eq. (A9) basically scales as $(L-N)^3$ (which is the cost of the matrix inversion involved). Depending on the relative sizes of L and N one of these two steps is dominant.

3. F matrices

In this section explicit expressions for the matrices **F** and $\tilde{\mathbf{F}}$ are given [see Eqs. (13) and (14)]. Following Eq. (8), we denote the propagating and evanescent modes of the ideal wire by $\mathbf{u}_m$, $m=1,\ldots,M$, where $M<N_{\mathrm{rs}}$ and N_{rs} is the dimension of the vectors. For clarity of notation we omit the labels $\pm$ for right and left going modes here. As in Eq. (8) we form the $N_{\mathrm{rs}}\times M$ matrix

$$\mathbf{U} = (\mathbf{u}_1 \cdots \mathbf{u}_M) \tag{A10}$$

$$= \begin{pmatrix} u_{11} & \ldots & u_{1M} \\ \vdots & & \vdots \\ u_{N_{\mathrm{rs}}1} & \ldots & u_{N_{\mathrm{rs}}M} \end{pmatrix}. \tag{A11}$$

The mode vectors $\mathbf{u}_m$ are in general nonorthogonal and we can form the $M\times M$ (positive definite) overlap matrix with elements

$$S_{mn} = \mathbf{u}_m^{\dagger}\mathbf{u}_n \equiv \langle \mathbf{u}_m|\mathbf{u}_n\rangle. \tag{A12}$$

This allows us to construct the dual basis $\tilde{\mathbf{u}}_m$, $m=1,\ldots,M$,

$$\tilde{\mathbf{u}}_m = \sum_{n=1}^{M} S_{mn}^{-1}\mathbf{u}_n, \tag{A13}$$

with properties

$$\langle \tilde{\mathbf{u}}_m|\mathbf{u}_n\rangle = \langle \mathbf{u}_m|\tilde{\mathbf{u}}_n\rangle = \delta_{mn}. \tag{A14}$$

Now define the $M\times N_{\mathrm{rs}}$ matrix

$$\tilde{\mathbf{U}} = (\tilde{\mathbf{u}}_1 \cdots \tilde{\mathbf{u}}_M)^{\dagger} = \begin{pmatrix} \tilde{u}_{11}^{*} & \ldots & \tilde{u}_{N_{\mathrm{rs}}1}^{*} \\ \vdots & & \vdots \\ \tilde{u}_{1M}^{*} & \ldots & \tilde{u}_{N_{\mathrm{rs}}M}^{*} \end{pmatrix}. \tag{A15}$$

$\tilde{\mathbf{U}}$ is called the pseudoinverse of **U**; note that $\tilde{\mathbf{U}}\mathbf{U}=\mathbf{I}_M$, where $\mathbf{I}_M$ is the $M\times M$ identity matrix.[55]

Defining the matrix

$$\mathbf{F} = \mathbf{U}\boldsymbol{\Lambda}\tilde{\mathbf{U}}, \tag{A16}$$

it is easy to show that it is a solution to Eq. (13). **F** is in fact a matrix that projects onto the space spanned by the modes, as is easily demonstrated by writing Eq. (A16) as

$$\mathbf{F} = \sum_{m=1}^{M} |\mathbf{u}_m\rangle\lambda_m\langle\tilde{\mathbf{u}}_m|, \tag{A17}$$

making use of Eqs. (11) and (A10)–(A15). In a similar way a solution to Eq. (14) is formed by

$$\tilde{\mathbf{F}} = \mathbf{U}\mathbf{\Lambda}^{-1}\tilde{\mathbf{U}} = \sum_{m=1}^{M} |\mathbf{u}_m\rangle \lambda_m^{-1} \langle \tilde{\mathbf{u}}_m|. \tag{A18}$$

Note that $\tilde{\mathbf{F}} = \mathbf{F}^{-1}$ only if $M = N_{\mathrm{rs}}$, but since $M \leqslant N \times W_x \times W_y < N_{\mathrm{rs}}$ (see the previous section) this will never be the case.

4. Scattering problem

The scattering problem is described by Eq. (26). It is conveniently written in matrix form as

$$\begin{pmatrix} \mathbf{A}_0 & \mathbf{B}^\dagger & 0 & \dots & 0 \\ \mathbf{B} & \mathbf{A}_1 & \mathbf{B}^\dagger & \dots & 0 \\ 0 & \mathbf{B} & \mathbf{A}_2 & \dots & 0 \\ \vdots & \vdots & \vdots & \vdots & \vdots \\ 0 & 0 & 0 & \dots & \mathbf{A}_{S+1} \end{pmatrix} \begin{pmatrix} \mathbf{C}_0 \\ \mathbf{C}_1 \\ \mathbf{C}_2 \\ \vdots \\ \mathbf{C}_{S+1} \end{pmatrix} = \begin{pmatrix} \mathbf{D} \\ 0 \\ 0 \\ \vdots \\ 0 \end{pmatrix}, \tag{A19}$$

with

$$\mathbf{A}_0 = E\mathbf{I} - \tilde{\mathbf{H}}_0,$$

$$\mathbf{A}_i = E\mathbf{I} - \mathbf{H}_i,\ i = 1, \dots, S,$$

$$\mathbf{A}_{S+1} = E\mathbf{I} - \tilde{\mathbf{H}}_{S+1},$$

$$\mathbf{C}_0 = \mathbf{U}_{\mathrm{L}}(+) + \mathbf{U}_{\mathrm{L}}(-)\mathbf{R},$$

$$\mathbf{C}_{S+1} = \mathbf{U}_{\mathrm{R}}(+)\mathbf{T},$$

$$\mathbf{D} = \mathbf{Q}\mathbf{U}_{\mathrm{L}}(+). \tag{A20}$$

All the blocks $\mathbf{A}$–$\mathbf{D}$ are $N_{\mathrm{rs}} \times N_{\mathrm{rs}}$ matrices. Equation (A19) represents a set of linear equations, which can be solved directly using a standard algorithm. However, the dimension of this problem is $N_{\mathrm{tot}} = N_{\mathrm{rs}}(S+2)$, which can be rather large. Since the computing cost scales as N_{tot}^3 the direct route is not very practical.

It is however quite straightforward to construct an algorithm for which the computing cost scales as $N_{\mathrm{rs}}^3 S$, i.e., only linearly with the size S of the scattering region. One has to make optimal use of the block tridiagonal form of the matrix in Eq. (A19). The algorithm is a block form of Gaussian elimination. The first (and most time consuming) step of this algorithm is transforming the matrix into upper block triangular form by iteration:

$$\mathbf{A'}_0 = \mathbf{A}_0, \mathbf{D'}_0 = \mathbf{D},$$

$$\left.\begin{aligned} \mathbf{A'}_i &= \mathbf{A}_i - \mathbf{B}\mathbf{A'}_{i-1}^{-1}\mathbf{B}^\dagger, \\ \mathbf{D'}_i &= -\mathbf{B}\mathbf{A'}_{i-1}^{-1}\mathbf{D'}_{i-1}, \end{aligned}\right\} i = 1, \dots, S+1. \tag{A21}$$

The inverse matrices $\mathbf{A'}_{i-1}^{-1}$ in this algorithm are actually not needed explicitly. Instead at each step one solves the sets of linear equations

$$\mathbf{A'}_{i-1}\tilde{\mathbf{B}}_i = \mathbf{B}^\dagger,\ \mathbf{A'}_{i-1}\tilde{\mathbf{D}}_i = \mathbf{D'}_{i-1}, \tag{A22}$$

by a standard algorithm, i.e., LU decomposition of $\mathbf{A'}_{i-1}$ followed by back substitution, to obtain the matrices $\tilde{\mathbf{B}}_i$ and $\tilde{\mathbf{D}}_i$.[55] This allows the steps in Eq. (A21) to be rewritten as

$$\mathbf{A'}_i = \mathbf{A}_i - \mathbf{B}\tilde{\mathbf{B}}_i,\ \mathbf{D'}_i = -\mathbf{B}\tilde{\mathbf{D}}_i. \tag{A23}$$

The solution to Eq. (A19) can now be found by back substitution

$$\mathbf{C}_{S+1} = \mathbf{A'}_{S+1}^{-1}\mathbf{D'}_{S+1},$$

$$\mathbf{C}_i = \tilde{\mathbf{D}}_{i+1} - \tilde{\mathbf{B}}_{i+1}\mathbf{C}_{i+1},\ i = S, \dots, 0. \tag{A24}$$

Again one does not need $\mathbf{A'}_{S+1}^{-1}$ explicitly, but as in Eq. (A22) one can solve the equivalent set of linear equations. The reflection and transmission matrices $\mathbf{R}$ and $\mathbf{T}$ can be extracted using the special form of the matrices $\mathbf{C}_0$ and $\mathbf{C}_{S+1}$, [see Eq. (A20)].

Very often one is interested only in the transmission matrix. In that case one uses only the first step of the back substitution, Eq. (A24), which can be written as

$$\mathbf{A'}_{S+1}\mathbf{U}_{\mathrm{R}}(+)\mathbf{T} = \mathbf{D'}_{S+1}. \tag{A25}$$

This is a set of linear equations for the transmission probability amplitudes $\mathbf{T}$, which can be solved using standard numerical techniques.[55]

The time consuming steps consist of solving Eq. (A22), the computing costs of which scale as N_{rs}^3.[56] Using Eq. (A23) in Eq. (A21) requires performing $S+1$ of such steps and subsequently solving Eq. (A25) scales as N_{rs}^3. Note that the full algorithm scales linearly with the size S of the scattering region.

5. Velocities

In this section we give a short derivation of the expression for the velocities, Eq. (28). It is straightforward to show that the vectors $\mathbf{u}_m$ of Eq. (8) are a solution of the quadratic eigenvalue equation

$$\lambda_m(E\mathbf{I} - \mathbf{H})\mathbf{u}_m + \mathbf{B}\mathbf{u}_m + \lambda_m^2\mathbf{B}^\dagger\mathbf{u}_m = 0. \tag{A26}$$

This quadratic eigenvalue equation of dimension N_{rs} is completely equivalent to the linear problem of dimension $2N_{\mathrm{rs}}$ of Eq. (7). If $\mathbf{u}_m$ is a right eigenvector of Eq. (A26) belonging to the eigenvalue λ_m, then by complex conjugation of this equation one shows that $\mathbf{u}_m^\dagger$ is a left eigenvector belonging to the eigenvalue $1/\lambda_m^*$. For a propagating state, $|\lambda_m| = 1$, so $\lambda_m = 1/\lambda_m^*$, which means that these left and right eigenvectors belong to the same eigenvalue.

We now start from

$$\lambda_m\mathbf{u}_m^\dagger(E\mathbf{I} - \mathbf{H})\mathbf{u}_m + \mathbf{u}_m^\dagger\mathbf{B}\mathbf{u}_m + \lambda_m^2\mathbf{u}_m^\dagger\mathbf{B}^\dagger\mathbf{u}_m = 0, \tag{A27}$$

and take the derivative d/dE of this expression. All the terms with $d\mathbf{u}_m/dE$ and $d\mathbf{u}_m^\dagger/dE$ drop out, because $\mathbf{u}_m$ and $\mathbf{u}_m^\dagger$ obey Eq. (A26) and its complex conjugate, respectively. The

remaining terms can be collected and slightly rewritten using Eq. (A26); the result is

$$\frac{d\lambda_m}{dE}(\lambda_m^{-1}\mathbf{u}_m^\dagger \mathbf{B}\mathbf{u}_m - \lambda_m \mathbf{u}_m^\dagger \mathbf{B}^\dagger \mathbf{u}_m) + \lambda_m \mathbf{u}_m^\dagger \mathbf{u}_m$$

$$= -2i\frac{d\lambda_m}{dE}\,\mathrm{Im}(\lambda_m \mathbf{u}_m^\dagger \mathbf{B}^\dagger \mathbf{u}_m) + \lambda_m = 0, \qquad \text{(A28)}$$

where the last line is obtained by making use of $\lambda_m^{-1}=\lambda_m^*$ and the fact that the vectors are normalized, $\mathbf{u}_m^\dagger \mathbf{u}_m = 1$. Equation (A28) yields an expression for $d\lambda_m/dE$. For propagating states $\lambda_m = e^{ik_x a_x}$ and thus

$$\frac{dk_x}{dE} = \frac{1}{ia_x\lambda_m}\frac{d\lambda_m}{dE}. \qquad \text{(A29)}$$

The usual definition of the Bloch velocity $v_n = \hbar^{-1} dE/dk_x$ and the expression for $d\lambda_m/dE$ extracted from Eq. (A28) then give the expression for the velocity of Eq. (28).

*Corresponding author. Email address: g.brocks@tn.utwente.nl; URL: http://www.tn.utwente.nl/cms

[1] N. Agraït, A. Levy Yeyati, and J. M. van Ruitenbeek, Phys. Rep. **377**, 81 (2003).

[2] M. Büttiker, Y. Imry, R. Landauer, and S. Pinhas, Phys. Rev. B **31**, 6207 (1985).

[3] T. N. Todorov, G. A. D. Briggs, and A. P. Sutton, J. Phys.: Condens. Matter **5**, 2389 (1993).

[4] K. Nicolić and A. MacKinnon, Phys. Rev. B **50**, 11 008 (1994).

[5] M. P. Samanta, W. Tian, S. Datta, J. I. Henderson, and C. P. Kubiak, Phys. Rev. B **53**, R7626 (1996).

[6] E. G. Emberly and G. Kirczenow, Phys. Rev. B **58**, 10 911 (1998).

[7] K. Hirose and M. Tsukada, Phys. Rev. Lett. **73**, 150 (1994); Phys. Rev. B **51**, 5278 (1995).

[8] N. D. Lang, Phys. Rev. B **52**, 5335 (1995); Phys. Rev. Lett. **79**, 1357 (1997).

[9] M. Di Ventra, S. T. Pantelides, and N. D. Lang, Phys. Rev. Lett. **84**, 979 (2000).

[10] H. J. Choi and J. Ihm, Phys. Rev. B **59**, 2267 (1999).

[11] Y. G. Yoon, M. S. C. Mazzoni, H. J. Choi, J. Ihm, and S. G. Louie, Phys. Rev. Lett. **86**, 688 (2001).

[12] S. Datta, *Electronic Transport in Mesoscopic Systems* (Cambridge University Press, Cambridge, U.K., 1995).

[13] Y. Xue, S. Datta, and M. A. Ratner, J. Chem. Phys. **115**, 4292 (2001); P. S. Damle, A. W. Ghosh, and S. Datta, Phys. Rev. B **64**, 201403 (2001).

[14] J. Taylor, H. Guo, and J. Wang, Phys. Rev. B **63**, 245407 (2001).

[15] M. Buongiorno Nardelli, J.-L. Fattebert, and J. Bernholc, Phys. Rev. B **64**, 245423 (2001).

[16] J. J. Palacios, A. J. Pérez-Jiménez, E. Louis, E. SanFabián, and J. A. Vergés, Phys. Rev. B **66**, 035322 (2002).

[17] J. Heurich, J. C. Cuevas, W. Wenzel, and G. Schön, Phys. Rev. Lett. **88**, 256803 (2002).

[18] M. Brandbyge, J. L. Mozos, P. Ordejón, J. Taylor, and K. Stokbro, Phys. Rev. B **65**, 165401 (2002).

[19] K. S. Thygesen, M. V. Bollinger, and K. W. Jacobsen, Phys. Rev. B **67**, 115404 (2003).

[20] D. Wortmann, H. Ishida, and S. Blügel, Phys. Rev. B **66**, 075113 (2002).

[21] J. P. Vigneron and Ph. Lambin, J. Phys. A **12**, 1961 (1979); **13**, 1135 (1980).

[22] C. Berthod, F. Gagel, and K. Maschke, Phys. Rev. B **50**, 18 299 (1994); F. Gagel and K. Maschke, *ibid.* **52**, 2013 (1994).

[23] Y. Fujimoto and K. Hirose, Phys. Rev. B **67**, 195315 (2003).

[24] A. A. Starikov, I. I. Yakimenko, and K.-F. Berggren, Phys. Rev. B **67**, 235319 (2003).

[25] J. R. Chelikowsky, N. Troullier, and Y. Saad, Phys. Rev. Lett. **72**, 1240 (1994).

[26] J. R. Chelikowsky, N. Troullier, K. Wu, and Y. Saad, Phys. Rev. B **50**, 11 355 (1994).

[27] F. Gygi and G. Galli, Phys. Rev. B **52**, R2229 (1995).

[28] T. Ando, Phys. Rev. B **44**, 8017 (1991).

[29] If one uses Green functions, one has to distinguish between retarded and advanced Green functions. This can be done by subtracting or adding a (small) imaginary number to the energy.

[30] K. Xia, P. J. Kelly, G. E. W. Bauer, and I. Turek, Phys. Rev. Lett. **89**, 166603 (2002).

[31] M. Zwierzycki, K. Xia, P. J. Kelly, G. E. W. Bauer, and I. Turek, Phys. Rev. B **67**, 092401 (2003).

[32] L. Molinari, J. Phys. A **30**, 983 (1997).

[33] H.-O. Kreiss, Math. Comput. **26**, 605 (1972).

[34] H. Brandén, Technical Report No. 2000-026, Department of Information Technology, Uppsala University, Uppsala, Sweden, 2000 (unpublished).

[35] The size of the scattering region does not have to be an integer multiple of the size of the cell in the leads. One can choose cells of a different size in the scattering region. One also chooses differently sized cells in the left and right leads in case the leads are different. We have not introduced cells of different size here in order not to complicate the notation, but the strategy for solving the scattering problem as outlined in Appendix A 4 also works in that case.

[36] *Handbook of Mathematical Functions*, edited by M. Abramowitz and I. A. Stegun (Dover, New York, 1965).

[37] L. D. Landau and E. M. Lifschitz, *Quantum Mechanics: Non-relativistic Theory* (Pergamon Press, Oxford, 1981), Sec. 25.

[38] S. Wolfram, Computer code MATHEMATICA, http://documents.wolfram.com

[39] C. S. Barrett, Acta Crystallogr. **9**, 671 (1956).

[40] A. A. Quong, A. A. Maradudin, R. F. Wallis, J. A. Gaspar, A. G. Aguiluz, and G. P. Alldredge, Phys. Rev. Lett. **66**, 743 (1991).

[41] N. Kobayashi, M. Brandbyge, and M. Tsukada, Phys. Rev. B **62**, 8430 (2000).

[42] J. Perdew and A. Zunger, Phys. Rev. B **23**, 5048 (1981).

[43] N. Troullier and J. L. Martins, Phys. Rev. B **43**, 1993 (1991). The *s* part of the pseudopotential for sodium, generated with a core radius $r_c = 2.95a_0$, is used as the local potential. Tests using a nonlocal pseudopotential with *s* and *p* parts gave a virtually identical electronic structure for bulk sodium, indicating that the

use of a local potential is a good approximation for sodium.

[44] J. Neugebauer and M. Scheffler, Phys. Rev. B **46**, 16 067 (1992).

[45] N. J. Fall, N. Binggeli, and A. Baldereschi, J. Phys.: Condens. Matter **11**, 2689 (1999).

[46] The number of cells S required for the scattering region of an n-atomic wire is approximately n_L+n_R+n, where n_L and n_R is the number of unit cells that define the surface regions of left and right electrodes. The number of grid points per cell is $N_{rs}=LW_yW_z=3456$.

[47] We have aimed at a high accuracy here, but coarser grids can give acceptable results. A spacing $h_{x,y,z}=0.80$, which gives $N_{rs}=L\times W_y\times W_z=5\times 20\times 20$grid points per cell, combined with a 6×6 $\mathbf{k}_\parallel$-point sampling gives a conductance that deviates less than 2×10^{-3} from the highly accurate results.

[48] A. Levy Yeyati, A. Martín-Rodero, and F. Flores, Phys. Rev. B **56**, 10 369 (1997).

[49] H.-S. Sim, H.-W. Lee, and K. J. Chang, Phys. Rev. Lett. **87**, 096803 (2001).

[50] P. Havu, T. Torsti, M. J. Puska, and R. M. Nieminen, Phys. Rev. B **66**, 075401 (2002).

[51] S. Tsukamoto and K. Hirose, Phys. Rev. B **66**, 161402 (2002).

[52] Y. J. Lee, M. Brandbyge, M. J. Puska, J. Taylor, K. Stockbro, and R. M. Nieminen, Phys. Rev. B **69**, 125409 (2004).

[53] K. S. Thygesen and K. W. Jacobsen, Phys. Rev. Lett. **91**, 146801 (2003).

[54] Somewhat surprisingly, the size of the even-odd oscillation is, however, quite sensitive to the accuracy of the sodium potential used as input for the transport calculations. Extracting this potential from a self-consistent ground state calculation requires the ground state energy to be converged at the scale of 10^{-6}–10^{-7} hartrees. A weaker convergence criterion of 10^{-5} hartrees yields a potential that can change the conductance by up to 5% and can even suppress the even-odd oscillation almost completely.

[55] G. Golub and C. F. van Loan, *Matrix Computations* (Johns Hopkins University Press, Baltimore, 1996).

[56] One can make use of the special form of the **H** and **B** matrices [cf. Eqs. (A1) and (A3)] to subdivide the blocks of the matrix in Eq. (A19). This can speed up the algorithm by an order of magnitude. However, the overall scaling still is as N_{rs}^3S.